Transition strengths between particle hole excitations in ^{95}Ru

E. Galindo, M. Hausmann, A. Jungclaus,* K. P. Lieb, and O. Yordanov†
II. Physikalisches Institut, Universität Göttingen, Bunsenstrasse 7-9, D-37073 Göttingen, Germany

I. P. Johnstone
Department of Physics, Queen's University, Ontario, Canada K7L 3N6

R. Schwengner
Institut für Kern- und Hadronenphysik, Forschungszentrum Rossendorf, D-01314 Dresden, Germany

A. Dewald, A. Fitzler, and O. Möller
Institut für Kernphysik, Universität zu Köln, D-50937 Köln, Germany

G. de Angelis, A. Gadea, T. Martinez, and D. R. Napoli
Istituto Nazionale di Fisica Nucleare, Laboratori Nazionali di Legnaro, I-35020 Legnaro, Italy

C. A. Ur‡
Istituto Nazionale di Fisica Nucleare, Sezione di Padova, I-35131 Padova, Italy
(Received 5 May 2003; published 18 February 2004)

High-spin states of ^{95}Ru have been populated using the ^{35}Cl+^{64}Zn reaction at a beam energy of 135 MeV. In a recoil-distance Doppler-shift experiment, the lifetimes or lifetime limits of 26 high-spin states have been measured, giving information on a total of 49 reduced transition strengths. The results are compared with shell-model calculations with different model spaces and residual interactions. Several families of states with defined proton and neutron seniorities are proposed. The $M1$ strengths in the negative-parity yrast sequence show a pronounced staggering which is reproduced by the shell-model calculations.

DOI: 10.1103/PhysRevC.69.024304 PACS number(s): 21.10.Tg, 21.10.Ky, 21.60.Cs, 27.60.+j

I. INTRODUCTION

Recent studies of the $N \approx 50$ nuclei near the doubly magic ^{100}Sn nucleus have given evidence of high-spin structures, which can be separated into substructures or "families" with rather well-defined proton and neutron seniorities [1–3]. In the frame of the spherical shell model these structures can be understood due to the interplay between $f_{5/2}, p_{3/2} \rightarrow g_{9/2}$ proton excitations, $g_{9/2} \rightarrow d_{5/2}, g_{7/2}, h_{11/2}$ neutron-core excitations, and recouplings of the $g_{9/2}$ valence protons. States within the same family are generally connected by strong $M1$ and moderate $E2$ transitions, while transitions connecting different families can be severely inhibited, giving rise to so-called seniority isomers. A detailed investigation of the reduced transition strengths provides the experimental basis for the contributions and interplay of the different configurations.

With one neutron in the $d_{5/2}$ orbital, high-spin states in the $N=51$ nuclei can be reached by a recoupling of the $g_{9/2}$ valence protons, by a $g_{9/2} \rightarrow d_{5/2}, g_{7/2}, h_{11/2}$ neutron (and/or proton) core excitation, such as in the $N=50$ nuclei, or by a $d_{5/2} \rightarrow h_{11/2}$ neutron valence excitation. The purpose of the present study was to extend the investigation to the $N=51$ nucleus ^{95}Ru, to search for further seniority isomers predicted by shell-model calculations, and to understand the nature of various energy gaps present in the high-spin scheme. For that reason, two shell-model calculations involving different classes of particle-hole excitations have been performed.

The high-spin level scheme of ^{95}Ru established by Ghugre and collaborators [4] was essentially confirmed in the present work, apart from some modifications which extend the levels up to spin $(43/2^+)$. Information about the lifetimes of the $17/2^+$ and $21/2^+$ states was previously reported in Ref. [4] and was used in the present analysis. A large number of picosecond lifetime limits was measured.

II. EXPERIMENT

High-spin states in ^{95}Ru were populated using the ^{64}Zn(^{35}Cl, $3pn$)^{95}Ru reaction at a beam energy of 135 MeV. The 1.0-mg/cm^2-thick ^{64}Zn foil (enriched to 99.8%) was bombarded with the $\sim$1 particle-nA ^{35}Cl beam provided by the XTU tandem accelerator of the INFN at Legnaro, Italy. The target was mounted in the Cologne plunger apparatus parallel to a 7-μm-thick stretched Au-stopper foil. Data were taken for 13 target-stopper distances between $x=20$ μm and 6117 μm. The γ radiation was detected using the GASP 4π Ge detector array with six neutron detectors placed in for-

*Present address: Dep. Fisica Teórica, Universidad Autónoma de Madrid and Instituto de Estructura de la Materia, Consejo Superior de Investigaciones Científicas, Madrid, Spain.

†Present address: GSI, D-64291 Darmstadt, Germany.

‡On leave from the National Institute for Physics and Nuclear Engineering, Bucharest, Romania.

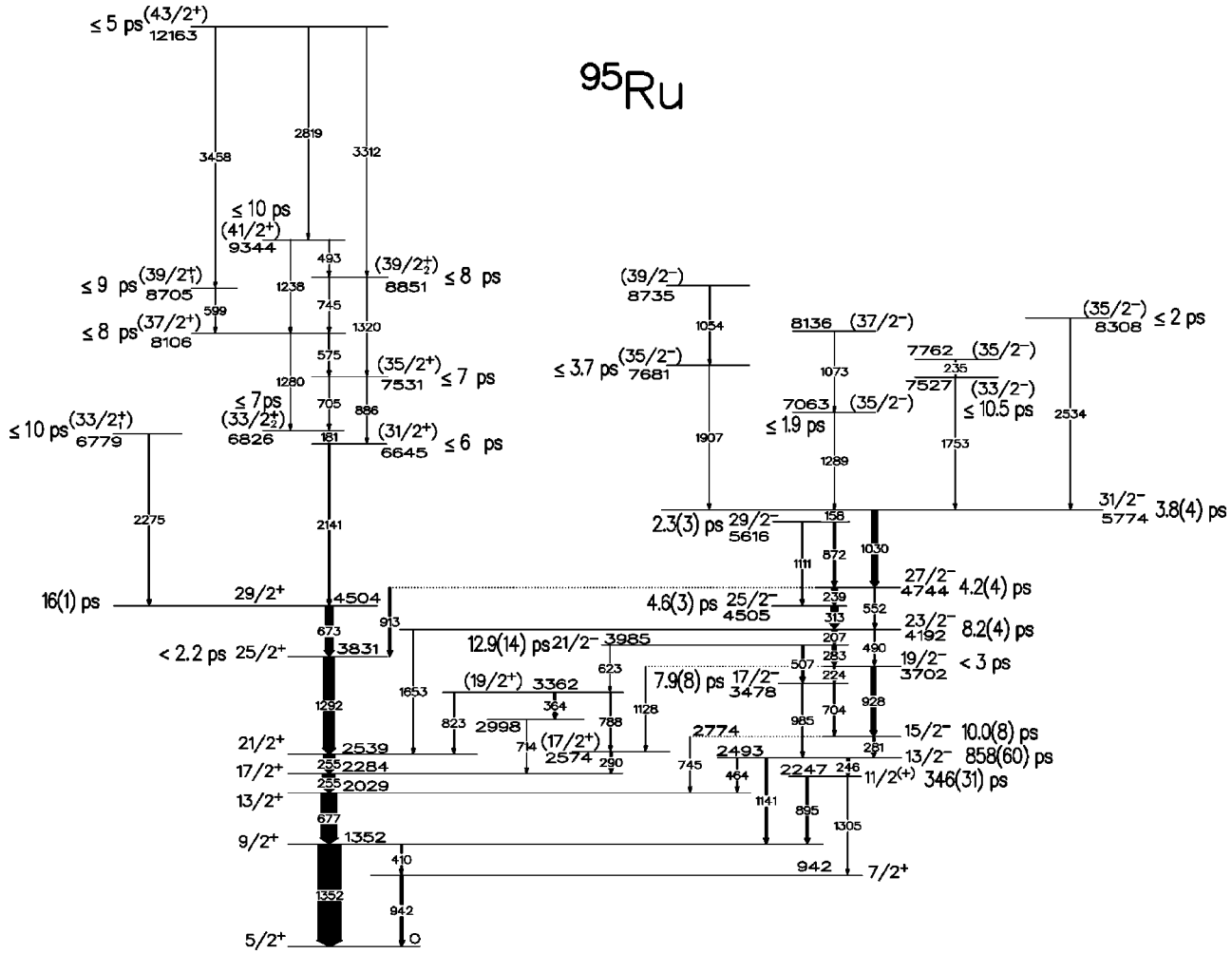

FIG. 1. Level scheme of ^{95}Ru as proposed and used in the present work.

ward direction. The 40 Ge detectors of GASP are arranged in seven rings at angles of 35°, 59°, 72°, 90°, 108°, 121°, and 145° with respect to the beam. The forward Ge ring was shifted away from the target by 4 cm and the backward Ge and BGO-rings were shifted by 5 cm in order to fit the plunger apparatus inside the array.

The recorded data were sorted into 49 different $\gamma\gamma$-coincidence matrices for each flight distance to be accumulated in all the seven detector rings and with gates set in all seven rings, too. Spectra in the 72°, 90°, and 108° rings were not analyzed because the small Doppler shifts observed under these angles do not allow for a clear separation between shifted and unshifted components of the γ rays of interest. The recoil velocity of $v/c=2.55(1)\%$ was deduced for ^{95}Ru in the present experiment. A more detailed description of the data taking and treatment can be found in Ref. [3].

III. RESULTS

A. The level scheme

The level scheme used in the present work and shown in Fig. 1 is based on the one previously published by Ghugre *et al.* [4] and modified here using the good counting statistics of the present experiment. As part of the checking of the level scheme, a gate was set on the 255-keV doublet transition $(21/2^+ \rightarrow 17/2^+ \rightarrow 13/2^+)$. The corresponding coincidence spectrum, which is shown in Fig. 2, contains several new high-energy transitions, giving evidence for the existence of states of higher spins. A second gate was then set on the 181-keV line $(33/2^+ \rightarrow 31/2^+)$ and again lines at 1280 keV, 1238 keV, 1320 keV, 2819 keV, 3312 keV, and 3458 keV were observed (Fig. 3). Tentative spin-parity assignments were made. Note that the presumed positive-parity yrast cascade above spin $29/2$ deviates from the level ordering proposed in Ref. [4]. With these modifications, the level scheme exhibits several interesting characteristics, given as follows.

(a) The $29/2^+$ level and the $5/2^+$ ground state are connected via an $E2$ cascade.

(b) The spin range $(41/2^+)-29/2^+$ exhibits a $\Delta I=1$ cascade with $E2$ crossover transitions.

(c) At negative parity the $13/2^-$ (2493 keV) state is connected to the $31/2^-$ (5774-keV) level via a $\Delta I=1$ cascade with $E2$ crossover transitions.

(d) As usual in shell-model structures, transitions of low energy (about 200 keV) and high energy (up to 3.3 MeV) are found close to each other along the cascades.

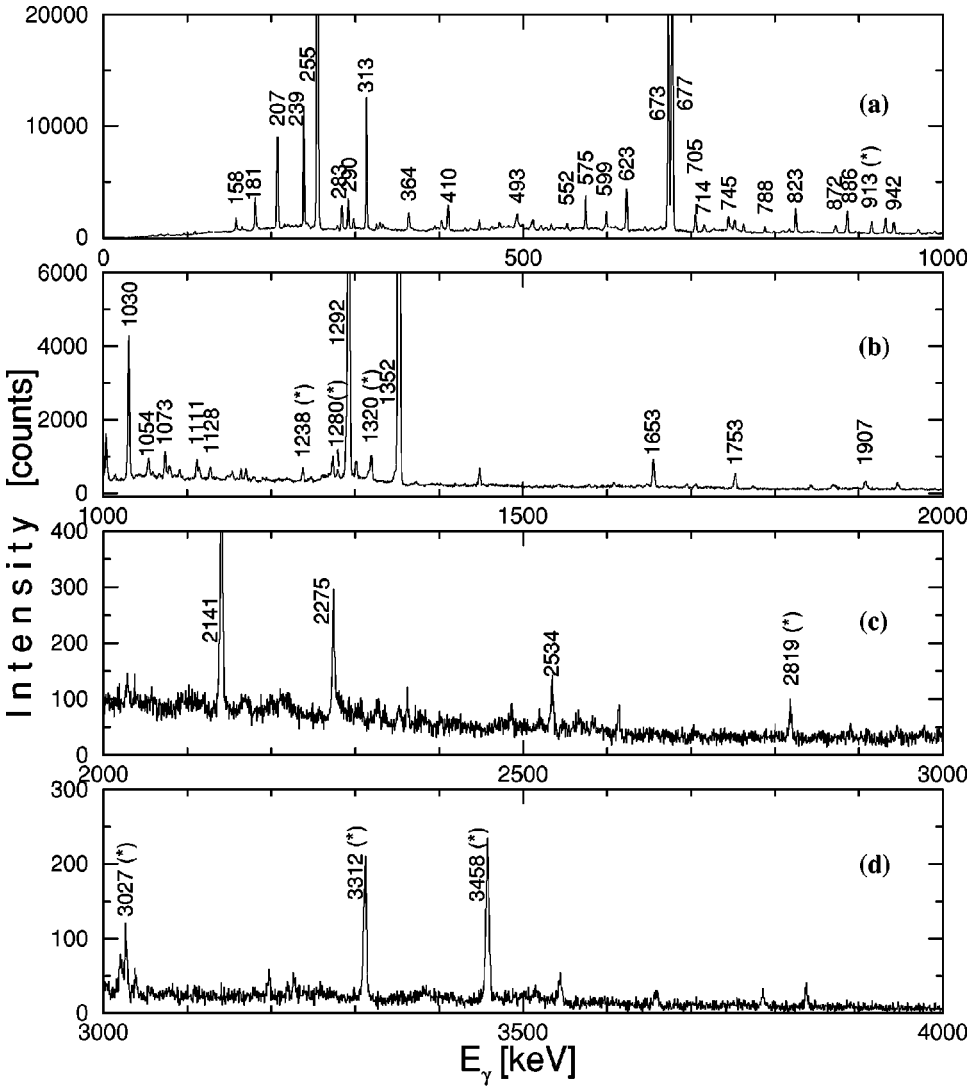

FIG. 2. γ-γ coincidence spectrum of ^{95}Ru by gating on the 255-keV transition. All the new transitions in the present work are marked with asterisks (*).

Moreover, this high-spin scheme permits us to identify the following four gaps of high-energy transitions: gap 1, between the $21/2^+$ (2539-keV) state and the $25/2^+$ (3831 -keV) state ($\Delta E = 1292$ keV); gap 2, between the $29/2^+$ (4504-keV) state and the $(31/2^+)$ (6645-keV) state ($\Delta E = 2141$ keV); gap 3, separating the $(41/2^+)$ (9344-keV) state and the $(43/2^+)$(12 163-keV) state ($\Delta E = 2819$ keV); and gap 4, above the $31/2^-$ (5774-keV) state ($\Delta E = 1289, 1753, 1907$, and 2534 keV). Each of these gaps appears to represent a fundamental change in the shell-model structure, as will be discussed below.

B. The DDCM analysis

The lifetime analysis of ^{95}Ru started using the differential decay curve method (DDCM) in the coincidence mode [5,6]. This method is suitable for the analysis of recoil-distance Doppler-shift experiments, especially in nuclei with shell-model structures, where the systematics of side-feeding times is unknown. DDCM fully avoids the influence of such side-feeding times. With DDCM a total of eight lifetimes between 2.3 and 350 ps was measured in ^{95}Ru. Some details of this analysis will be commented on below.

The $15/2^-$ state at 2774 keV is populated mainly via the 928-keV transition from the $19/2^-$ state at 3702 keV and by the 704-keV transition from the $17/2^-$ state at 3478 keV; it decays via the 745-keV and the 281-keV transitions. A suitable selection of gate and observed lines were the 928-keV (gate) and the 281-keV (observed) line. The 59° and 121° rings were not considered in the analysis because it was not possible to separate the flight components of the 281-keV and 283-keV transitions, both belonging to the same cascade. Therefore this analysis was performed taking only the 35° and 145° rings. The upper curve displayed in Fig. 4(a) refers to the intensity I_S of the stop component of the depopulating 281-keV γ ray when gating on the 928-keV flight peak. In the center of Fig. 4(a), the slope of the flight component intensity dI_F/dt for the 281-keV γ ray by gating on the 928-keV flight peak is shown. Finally the ratio τ

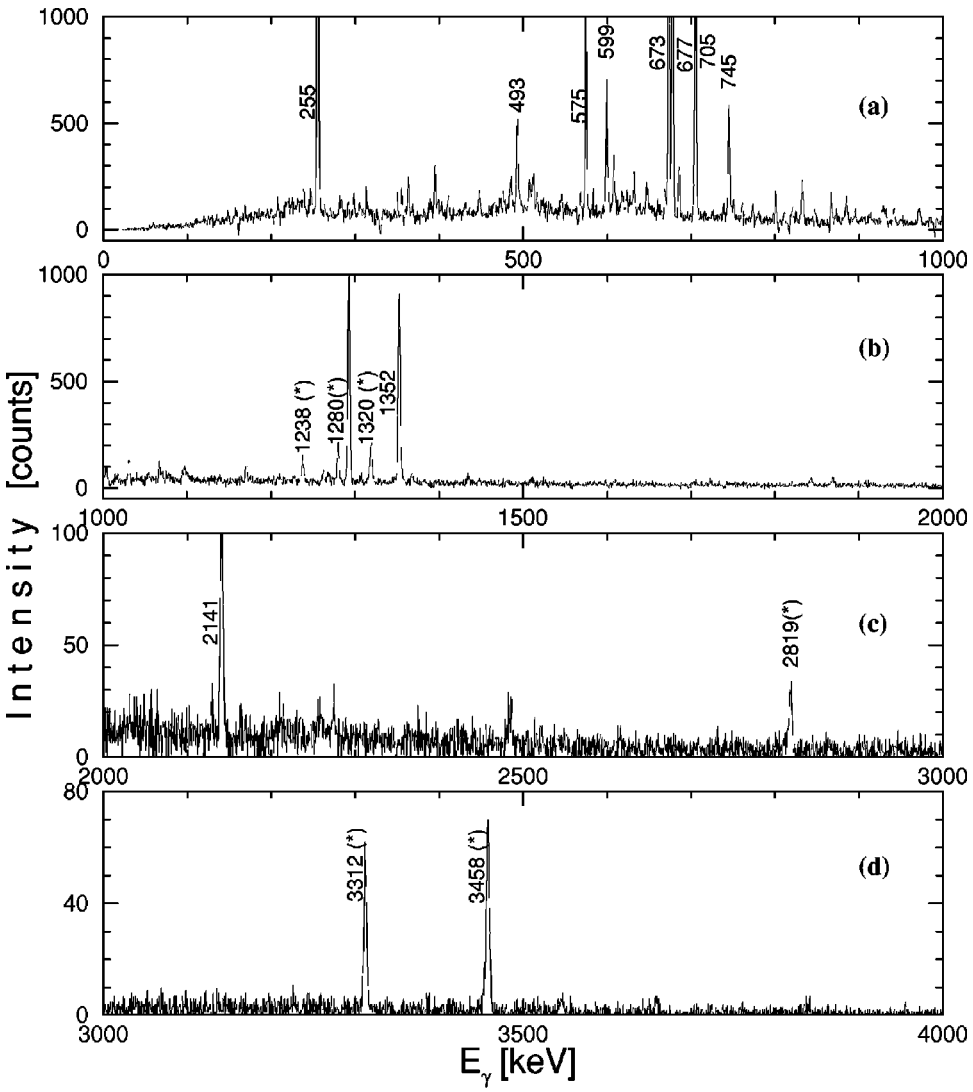

FIG. 3. γ-γ coincidence spectrum of ^{95}Ru by gating on the 181-keV transition. All the new transitions in this gate are marked with asterisks (*).

$=I_S/(dI_F/dt)$ is plotted in the lower part as a function of the flight distance, giving the mean lifetime $\tau(15/2^-)=10.0(8)$ ps.

A similar situation occurred for the $17/2^-$ (3478-keV) state. Here again only the more forward and backward angles were taken in the analysis. Figure 4(b) shows the deduced functions I_S and dI_F/dt of the decaying 704-keV γ ray in the gate on the flight component of the 224-keV feeding transition. The DDCM lifetime analysis referring to the $21/2^-$ state at 3985 keV is documented in Fig. 4(c). The gate was set on the 207-keV transition. From the I_S and dI_F/dt curves displayed in Fig. 4(c), the lifetime $\tau(21/2^-)=12.9(14)$ ps was adopted. With a gate set on the 313-keV feeder line we observed smooth curves of the stop and flight components of the 207-keV decay transition of the 4192-keV $23/2^-$ state shown in Fig. 4(d), giving $\tau(23/2^-)=8.2(4)$ ps.

Concerning negative-parity states, Figs. 5(a)–5(d) show the $I_S(x)$ and $dI_F(x)/dt$ curves and the lifetime values $\tau(x)$ for various γ-ray lines as a function of the recoil distance x, as well as the information about the observed line and gate, for the states $25/2^-$, $-29/2^-$, and for the state of assumed positive parity $11/2^{(+)}$ (2247 keV). The measured lifetimes with their respective information about gate and observed lines are summarized in Table I. Due to low intensities and/or contaminations, further DDCM lifetime measurements at positive parity were not possible.

C. The standard RDDS analysis

The low intensities of some observed and/or gate lines, as well as contamination with other lines did not allow a DDCM analysis in some cases, especially at high spin. In these cases standard decay curve analyses (RDDS) were performed. To this end, decay curves of γ transitions were determined in coincidence with intense lines at lower excitation energies. This method of analysis requires full information on the feeding scenario (lifetimes, intensities) and in particular on side-feeding times.

Figures 6 and 7 show the decay curves for the positive- and negative-parity cascades, respectively. Evidently, the

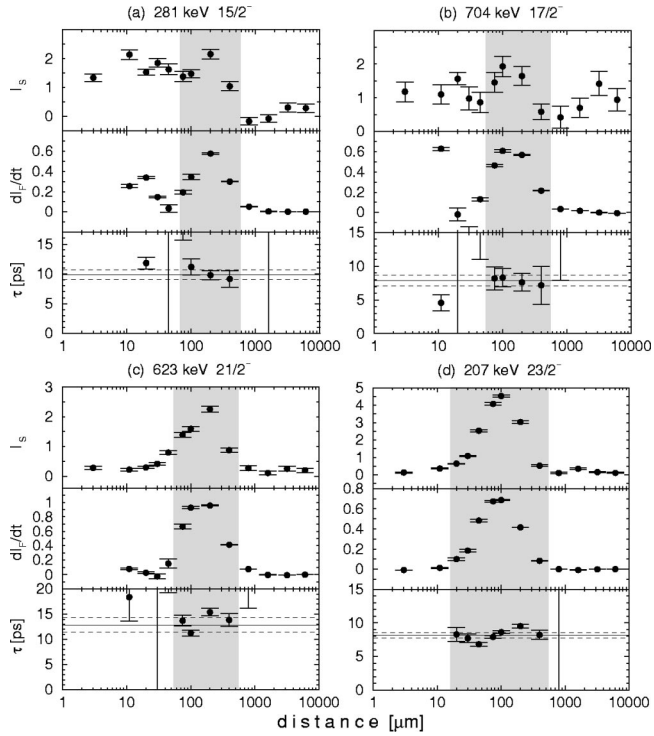

FIG. 4. DDCM analysis. Illustrated are the quantities I_s, dI_f/dt, and τ for the states $15/2^-$, $17/2^-$, $21/2^-$, and $23/2^-$. The considered region is indicated for each case.

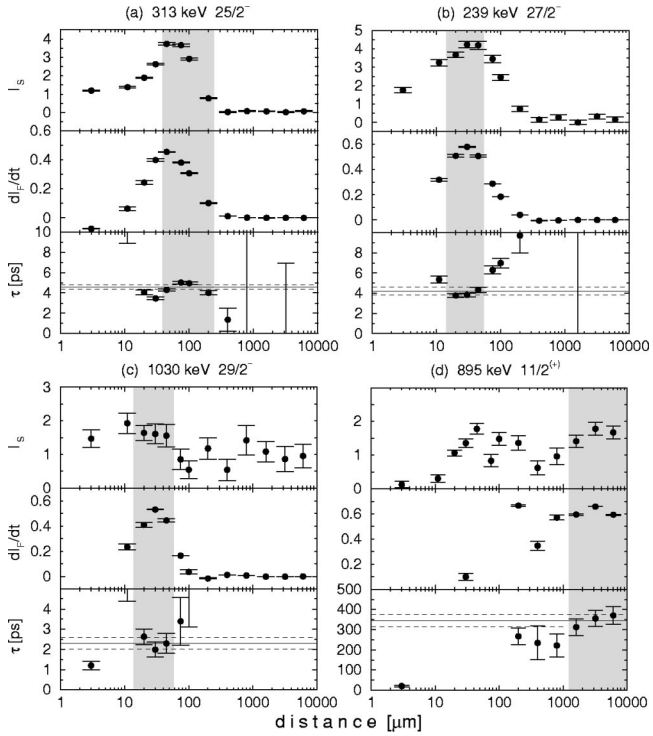

FIG. 5. DDCM analysis of the $25/2^-$, $-27/2^-$, $29/2^-$ and $11/2^{(+)}$ yrast states.

time structure at positive parity is dominated by the slow decays of the $21/2^+$ and $17/2^+$ states, through the 255-keV transitions, and at negative parity by the decay of the $13/2^-$ level. The 12 163-keV $(43/2^+)$ state decays via the 3458-keV, 2819-keV, and 3312-keV lines. The decay curve of the 3458-keV line was fitted to an exponential function giving an effective lifetime of $\tau_{eff}(43/2^+)=4.7(4)$ ps. As we can see in Fig. 6, the decay curves of the transitions in the spin range $(43/2^+)$ to $31/2^+$ appear very similar. This implies that the lifetimes of these intermediate states are rather small and therefore difficult to determine in a standard RDDS analysis. For all these intermediate states, we adopt upper lifetime limits deduced from the fitted effective lifetimes which are included in Table I.

The 4504-keV $29/2^+$ state is populated via the discrete transitions 2275 keV (15%) and 2141 keV (22%) and via continuum side feeding (SF) (63%). The lifetime analysis was carried out for the 673-keV line gated on the 255-keV line; the feeding scenario is sketched in Fig. 8(b). The side-feeding time τ_{SF} was considered as a free-fitting parameter and the lifetime and χ^2_{red} were calculated as a function of τ_{SF} [see Fig. 8(a)]. The adopted values of the lifetime $\tau(29/2^+)=16(1)$ ps and the side-feeding time τ_{SF} are the values for which χ^2_{red} reached a minimum.

A similar scenario was considered for the measurement of the lifetime of the 3831-keV $25/2^+$ state, which is populated via the 673-keV (65%) and the 913-keV line (15%) discrete feeders and via side feeding (20%) [see Fig. 8(d)]. For this state the fit procedure did not converge and gave only limits of the lifetime $\tau(25/2^+)<2.2$ ps and side-feeding time $\tau_{SF}(25/2^+)>1.7$ ps. No further RDDS measurements were possible at positive parity because the two isomeric states at 2284 keV and 2539 keV prevent us from measuring the lifetimes of the presumably shorter-lived lower members of this cascade.

The lowest observed state of negative parity, the 2493-keV 13/2− state, is populated via the 281-keV and 985-keV transitions. This state has a rather long lifetime and dominates the decay curves at negative parity as shown in Fig. 7. From the decay curves of the 1907 -keV (8%),
1289-keV (11%), 1753-keV (11%), and 2534-keV (4%) transitions on top of the negative-parity structure, the effective lifetimes summarized in Table I were found. With a 66% side feeding [$\tau_{SF}(31/2^-)=2.4(5)$ ps] and the feeding scenario of the 5774-keV $31/2^-$ state sketched in Fig. 9(b) we determined its lifetime as $\tau=3.8(4)$ ps.

D. Experimental transition strengths

With the information gained of 11 lifetimes and 15 lifetime limits and the branching ratios taken from Ref. [4] and the present $\gamma\gamma$-coincidence analysis, a total of 49 experimental reduced transition strengths $B(E2)$, $B(M1)$, $B(E1)$, and possibly $B(M2)$ were deduced in ^{95}Ru, which are listed in Table II. The $\Delta I=1$ transitions were considered to be of pure dipole character, i.e., $E2/M1$ mixing ratios $\delta=0$ were assumed. In the following analysis, the lifetimes of the isomeric $21/2^+$ and $17/2^+$ yrast states were adopted from a previous study [4], with values of 14.5(2) ns and 4.4(4) ns, respectively. For both parities the $E2$ transitions are moder-

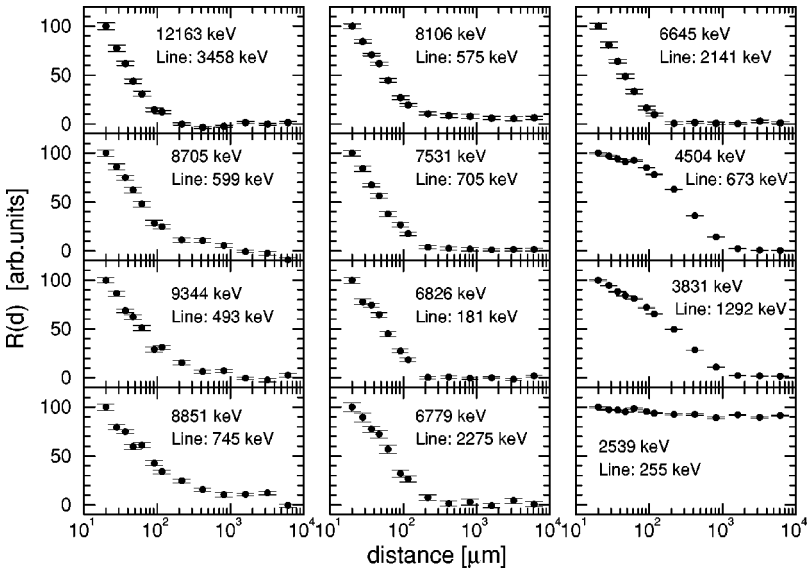

FIG. 6. Decay curve of the states at positive parity by gating on the 1352-keV line.

ately enhanced with $B(E2)$ values between 0.1 and 19 W.u. (Weisskopf units). In the case of the nonobserved $25/2^- \rightarrow 21/2^-$ transition, we estimated an upper $B(E2)$ limit assuming that the branching ratio of this transition has to be smaller than 5%. Few $B(M1)$ values at positive parity could be measured and only limits were gained in several cases. However, we note that above spin $31/2^+$ we encounter some strongly enhanced $B(M1)$. Within the negative-parity yrast cascade in the spin range $15/2^- - 31/2^-$ some $B(M1)$ values are fairly large (70–500 mW.u.), with the exception of the weak $17/2^- \rightarrow 15/2^-$ $M1$ (5.8 mW.u.) and $29/2^- \rightarrow 27/2^-$ (14 mW.u.) $M1$ strengths.

Let us now briefly discuss the 2247-keV $11/2$ state of nonassigned parity. Assuming positive parity for this state, the 246-keV line would be an $E1$ transition with $B(E1) = 16.1(16) \times 10^{-6}$ W.u., the 895-keV line an $M1$ transition with $B(M1) = 0.10(1)$ mW.u., and the 1305 keV an $E2$ transition with $B(E2) = 3.1(17)$ mW.u., All of these strengths are within the accepted ranges typical of this mass region. If we now assign negative parity to the 2247-keV state, the 246-keV transition would have $B(M1) = 0.10(1)$ mW.u., the 895 keV line $B(E1) = 1.6(2) \times 10^{-6}$ W.u., and the 1305-keV line $B(M2) = 0.19(9)$ W.u. Again, all these reduced transition strengths are acceptable. Therefore, the measured lifetime and decay branches of this state do not help fixing its parity. For the 3362-keV $19/2$ state the situation is similar: both transition strengths of $B(E1) = 14.4(32) \times 10^{-6}$ W.u. for the 623-keV transition, if its parity is positive, $B(M1) = 1.0(2)$ mW.u., if its parity is negative, are acceptable. The tentative assignments $I^\pi(2247) = 11/2^{(+)}$ and $I^\pi(3362) = 19/2^{(+)}$ are suggested by the shell-model calculations, which will now be discussed.

IV. INTERPRETATION IN THE FRAME OF THE SHELL MODEL

A. Classification of particle-hole excitations

The nucleus ^{95}Ru has six valence protons and a single valence neutron relative to the $N=50$ core ^{88}Sr. The simplest model space, $(g_{9/2}, p_{1/2})$ for protons and $d_{5/2}$ for the neutron outside this core, reaches states of positive parity up to $21/2^+$ with the $\pi^2(p_{1/2})\pi^4(g_{9/2}) \otimes \nu(d_{5/2})$ configuration (seniority $\upsilon_\nu = 3$, one broken $g_{9/2}$ pair). With a second broken $g_{9/2}$ proton pair, this configuration ($\upsilon = 5$) reaches a maximum spin of $29/2^+$. Similarly, states at negative parity, within the $\pi^2(p_{1/2})\pi^5(g_{9/2}) \otimes \nu(d_{5/2})$ configuration, reach up to spin

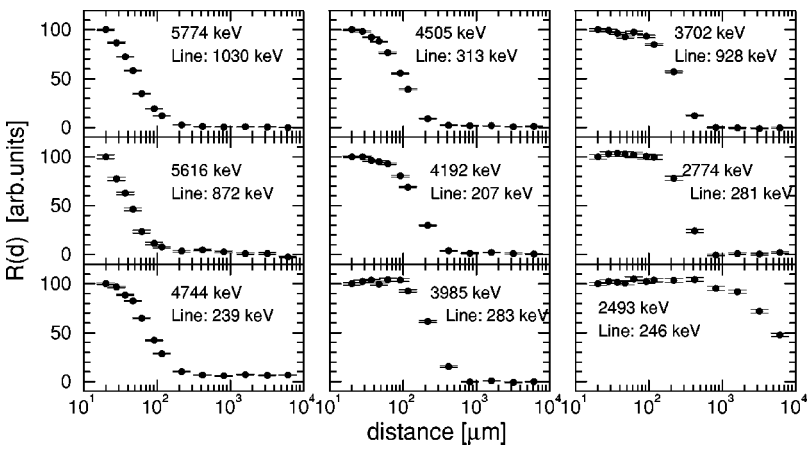

FIG. 7. Decay curve of the states at negative parity by gating on the 1352-keV line.

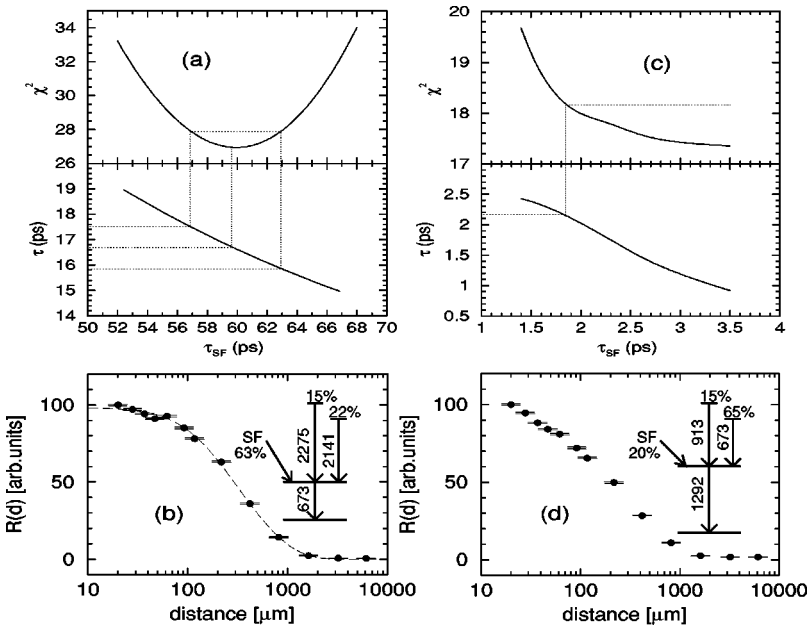

FIG. 8. Left: RDDS analysis of the $29/2^+$ (4504-keV) state. (a) The adopted values $\tau=16(1)$ ps and $\tau_{SF}=60(3)$ ps are values for which χ^2 reached a minimum. (b) Feeding scenario and $R(d)$ curve. Right: RDDS analysis for the $25/2^+$ (3831-keV) state. The decay curve and feeding scenario shown in (d) give only limits of lifetime ($\tau<2$ *ps*) and side-feeding time ($\tau_{SF}>2.5$ ps).

$31/2^-$ and seniority $v=7$. (In the following, we mention protons in the $p_{1/2}$ orbit only if they do not have seniority zero.) Shell-model states in ^{95}Ru within the larger spin range observed in the present work can be principally generated via three different mechanisms:

(a) Single proton excitations from the completely filled $p_{3/2}$, $f_{5/2}$ subshells into the $g_{9/2}$ orbit. The $\pi^{-1}(f_{5/2})\pi^5(g_{9/2})\otimes\nu(d_{5/2})$ and $\pi^{-1}(f_{3/2})\pi^5(g_{9/2})\otimes\nu(d_{5/2})$ $v=7$ configurations reach maximum spins of $35/2^-$ and $33/2^-$, respectively.

(b) Breaking of the neutron core by exciting a neutron from the $g_{9/2}$ into the $d_{5/2}$ orbital. This $v=7$ excitation allows a maximum spin of $41/2^+$ within the configuration $\pi^4(g_{9/2})\otimes\nu^{-1}(g_{9/2})\nu^2(d_{5/2})$. This structure in combination with a $p_{1/2}\rightarrow g_{9/2}$ proton "switch" permits to reach the spin $43/2^-$ and seniority $v=9$.

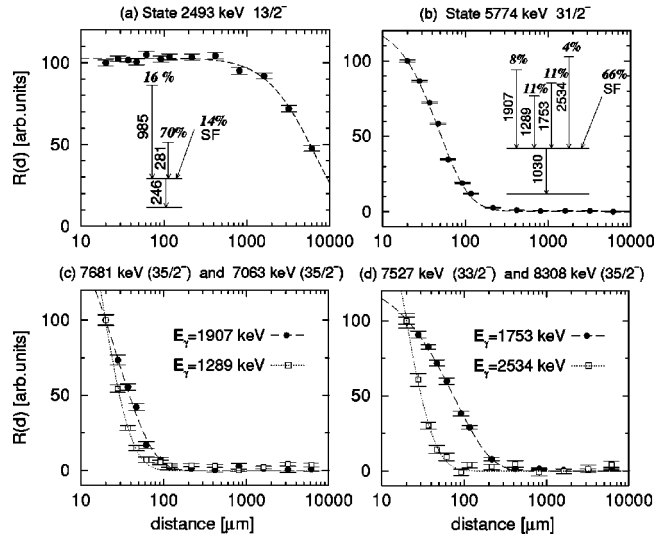

FIG. 9. RDDS analysis of the (a) $13/2^-$ (2493-keV) and (b) $31/2^-$ (5774-keV) states. (c) and (d) show the decay curves of the highest spin states in the negative parity, which populate the $31/2^-$ state.

(c) Neutron valence excitation from the $d_{5/2}$ orbit into the $h_{11/2}$ orbit with or without simultaneous $p_{1/2}\rightarrow g_{9/2}$ proton excitation. The $\pi^4(g_{9/2})\otimes\nu(h_{11/2})$ configuration provides a maximum spin of $35/2^-$ (seniority $v=5$), while the $\pi^{-1}(p_{1/2})\pi^5(g_{9/2})\otimes\nu(h_{11/2})$ wave function $v=7$ reaches up to $37/2^+$.

Previous shell-model calculations of ^{95}Ru by Ghugre *et al.* [4] performed with the code OXBASH [7] using the two-body matrix elements from Gloeckner [8] considered the core ^{88}Sr($Z=38, N=50$) with protons occupying the $(p_{1/2}, g_{9/2})$ orbits and a valence neutron in the $d_{5/2}$ or $s_{1/2}$ orbits. As mentioned before, the maximum spins are $29/2^+$ and $31/2^-$. The similar spacings between the positive-parity levels in ^{95}Ru (up to spin $29/2^+$) and ^{94}Ru (up to spin 12^+) are the basis for this interpretation. Negative-parity states are simply reached by a $p_{1/2}\rightarrow g_{9/2}$ proton excitation ($\leqslant 31/2^-$). Based on the similarity of the yrast sequences of ^{94}Ru and ^{95}Ru, Ghugre *et al.* suggested at higher spins a weak-coupling scheme of a $d_{5/2}$ neutron coupled to an excited ^{94}Ru core, $^{94}\mathrm{Ru}\otimes\nu(d_{5/2})$. In spite of a reasonably good agreement between the experimental and calculated level schemes, this model does not reproduce our proposed level scheme at high spins, because it does not provide an explanation of the gap 3 between the $(41/2^+)$ and $(43/2^+)$ states. Unfortunately, no transition strengths from this calculation have been reported.

On the other hand, these previous studies in ^{94}Ru and ^{95}Rh suggest that a $g_{9/2}\rightarrow d_{5/2}$ neutron-core excitation coupled to valence proton configurations has to be taken into account in order to describe the high-spin states. Recent lifetime and magnetic moment studies in the $N=50$ isotones ^{93}Tc, ^{94}Ru, and ^{95}Rh [1–3,9] have shown that, indeed, such neutron-core excitations are important at intermediate spins (B), but that they compete with proton excitations (A). For that reason, the structures of individual states cannot be determined on the basis of level energies only [1,2,9]. As different particle-hole excitations can compete with each other at these higher spins, it appears useful to consider their influence separately.

TABLE I. Lifetimes of excited states in ^{95}Ru as obtained in this work. The method used in the analysis is specified in the third column.

E_x (keV)	I^π	Method/Gate (keV)	E_γ (keV)	τ (ps)	τ_{SF} (ps)	τ_{adopted} (ps)
Positive parity						
2247	$11/2^{(+)}$	DDCM/246	895	346(31)		346(31)
2284	$17/2^+$					4.4(4) ns[a]
2539	$21/2^+$					14.5(2) ns[a]
3831	$25/2^+$	RDDS	1292	<2.2	>1.7	<2.2
4504	$29/2^+$	RDDS	673	16(1)	60(3)	16(1)
6645	$(31/2_1^+)$	RDDS	2141	$5.7(5)_{eff}$		$\leqslant 6$
6779	$(33/2_1^+)$	RDDS	2275	$9.3(5)_{eff}$		$\leqslant 10$
6826	$(33/2_2^+)$	RDDS	181	$6.3(4)_{eff}$		$\leqslant 7$
7531	$(35/2^+)$	RDDS	705	$6.3(7)_{eff}$		$\leqslant 7$
8106	$(37/2^+)$	RDDS	575	$6.9(7)_{eff}$		$\leqslant 8$
8705	$(39/2_1^+)$	RDDS	599	$8.2(9)_{eff}$		$\leqslant 9$
8851	$(39/2_2^+)$	RDDS	745	$7.5(5)_{eff}$		$\leqslant 8$
9344	$(41/2^+)$	RDDS	493	$8.9(10)_{eff}$		$\leqslant 10$
12163	$(43/2^+)$	RDDS	3458	$4.7(4)_{eff}$		$\leqslant 5$
Negative parity						
2493	$13/2^-$	RDDS	246	858(60)	152(42)	858(60)
2774	$15/2^-$	DDCM/928	281	10.0(8)		10.0(8)
3478	$17/2^-$	DDCM/224	704	7.9(8)		7.9(8)
3702	$19/2^-$	RDDS	928	<3.0		<3.0
3985	$21/2^-$	DDCM/207	623	12.9(14)		12.9(14)
4192	$23/2^-$	DDCM/313	207	8.2(4)		8.2(4)
4505	$25/2^-$	DDCM/239	313	4.6(3)		4.6(3)
4744	$27/2^-$	DDCM/1030	239	4.2(4)		4.2(4)
5616	$29/2^-$	DDCM /158	872	2.3(3)		2.3(3)
5774	$31/2^-$	RDDS	1030	3.8(4)	2.4(5)	3.8(4)
7063	$35/2_1^-$	RDDS	1289	$1.8(1)_{eff}$		$\leqslant 2$
7527	$33/2^-$	RDDS	1753	$10.2(3)_{eff}$		$\leqslant 11$
7681	$35/2_2^-$	RDDS	1907	$3.5(2)_{eff}$		$\leqslant 4$
8308	$35/2_3^-$	RDDS	2534	$1.9(1)_{eff}$		$\leqslant 2$

[a]Literature value taken from Ref. [4].

B. The shell-model calculations SM-I

The mechanism of generating high-spin states without neutron-core excitations but via a $\nu(d_{5/2}) \rightarrow \nu(h_{11/2})$ excitation (C) is discussed in the present section. These calculations were carried out using an ^{88}Sr core and a model space $(p_{1/2}, g_{9/2})$ for protons and $(d_{5/2}, s_{1/2}, d_{3/2}, g_{7/2}, h_{11/2})$ for neutrons. Considering thus a $d_{5/2} \rightarrow h_{11/2}$ neutron excitation (with or without a $p_{1/2} \rightarrow g_{9/2}$ proton "switch"), one reaches maximum spins of $35/2^-$ or $37/2^+$. This first set of calculations will be denoted in the following as SM-I.

The effective interactions used were determined by least-squares fits reproducing the spectra of $N=51$ nuclei [10], with the Perez interaction [11] (Coulomb corrected for protons) used for the matrix elements involving the $h_{11/2}$ orbit. The $J=2$ and $J=3$ $(p_{1/2}, d_{5/2})$ proton-neutron matrix elements were set equal to -0.442 MeV and -0.249 MeV to give the correct 2^- and 3^- energies in ^{90}Y. For more details see Refs. [12,10]. The effective charges and g factors used in all the calculations were $e_\pi = 1.77e$ and $e_\nu = 1.44e$, $g_{\pi l} = 1.0$, $g_{\nu l} = 0$, $g_{\pi s} = +3.909$, and $g_{\nu s} = -2.678$ equivalent to a spin quenching factor of 0.7.

The experimental and calculated excitation energies are compared in Fig. 10 (for the transitions, see Fig. 1). The calculations reproduce the experimental finding that the yrast sequence from $5/2^+$ up to spin $29/2^+$ is preferentially of $E2$ character followed by $M1$ transitions. The agreement in energy is very good up to spin $37/2^+$ and the gap between $29/2^+$ and $31/2^+$, the 2141-keV transition, is nicely reproduced. The calculations do not reach up to spin $41/2^+$ and thus do not explain the second gap in energy. In general, at positive parity the agreement is good for the yrast states, but not at all for the $19/2_2^+$ and $(33/2_2^+)$ yrare states. The agreement for the energy of the $37/2^+$ state suggests principally an $h_{11/2}$ neutron state configuration. The calculations also predict the assignment of $17/2_2^+$ for the 2574-keV state and

TABLE II. Experimental and calculated (SM-I and SM-II) transition strengths in ^{95}Ru. For the experimental transition strengths we assumed $\delta(E2/M1)=0$ for all $\Delta I=1$ transitions.

State	Transition				$B(E2)$ (W.u.)			$B(M1)$ (mW.u.)			$B(E1)$ (μW.u.)
E_x (keV)	I_i^π	I_f^π	E_γ (keV)	b (%)	Expt.	SM-I	SM-II	Expt.	SM-I	SM-II	Expt.
Positive parity											
2247	$11/2^{(+)}$	$7/2^+$	1305	14(4)	0.003(1)	1.1					
		$9/2^+$	895	86(4)				0.10(1)			
2284	$17/2^+$	$13/2^+$	255	100	6.7(6)	2.3	3.9				
2539	$21/2^+$	$17/2^+$	255	100	2.03(3)	2.1	3.7				
3831	$25/2^+$	$21/2^+$	1292	100	>4	7.7	9.5				
4504	$29/2^+$	$25/2^+$	673	100	14.3(9)	5.1	6.8				
6645	$(31/2^+)$	$29/2^+$	2141	100		0.21		$\geqslant$0.54	0.09	0.03	
6779	$(33/2_1^+)$	$29/2^+$	2275	100	$\geqslant$0.05	0.01					
6826	$(33/2_2^+)$	$(31/2^+)$	181	100		0.03		$\geqslant$760	4.3	43	
7531	$(35/2^+)$	$(31/2^+)$	886	58(6)	$\geqslant$4.8	0.05	10.1				
		$(33/2^+)$	705	42(6)		0.34		$\geqslant$5.4	3.8	592	
8106	$(37/2^+)$	$(33/2^+)$	1280	7(5)	$\geqslant$0.08	5.5	9.6				
		$(35/2^+)$	575	93(5)		1.8		$\geqslant$19	134	530	
8705	$(39/2_1^+)$	$(37/2^+)$	599	100				$\geqslant$17		288	
8851	$(39/2_2^+)$	$(35/2^+)$	1320	45(6)	$\geqslant$0.44						
		$(37/2^+)$	745	55(6)				$\geqslant$5.3			
9344	$(41/2^+)$	$(37/2^+)$	1238	29(4)	$\geqslant$0.32		6.0				
		$(39/2_2^+)$	493	71(4)				$\geqslant$19			
12163	$(43/2^+)$	$(39/2_1^+)$	3458	50(4)	$\geqslant$0.006		0.01				
		$(39/2_2^+)$	3312	18(4)	$\geqslant$0.003						
		$(41/2^+)$	2819	32(4)				$\geqslant$0.09		7.3	
Negative parity											
2493	$13/2^-$	$11/2^{(+)}$	246	44(3)				1.1(1)			16(2)
		$9/2^+$	1141	42(3)							0.51(5)[a]
		$13/2^+$	464	11(3)							0.6(2)
2774	$15/2^-$	$13/2^-$	281	95(2)		8.3		136(11)	480	485	
		$13/2^+$	745	5(2)							5.72(20)
3478	$17/2^-$	$15/2^-$	704	59(3)		0.01		6.8(8)	40	48	
		$13/2^-$	985	41(3)	1.77(22)	9.0	11.6				
3702	$19/2^-$	$(17/2^+)$	1128	6(2)							>6.1
		$15/2^-$	928	74(2)	>11	11.0	12.4				
		$17/2^-$	224	20(2)		5.2		>189	510	603	
3985	$21/2^-$	$19/2^-$	283	65(2)		0.11		76(9)	102	148	
		$17/2^-$	507	25(2)	18.3(25)	9.9	13.0				
		$19/2^+$	623	10(2)							15.1(34)
4192	$23/2^-$	$19/2^-$	490	13(3)	17.8(42)	11.4	13.8				
		$21/2^-$	207	74(3)		4.0		324(21)	515	642	
		$21/2^+$	1653	13(3)							1.64(27)
4505	$25/2^-$	$23/2^-$	313	100		1.0		226(15)	234	248	
4744	$27/2^-$	$25/2^-$	239	89(7)		2.5		494(61)	621	749	
		$23/2^-$	552	11(7)	16(10)	8.4	10.5				
5616	$29/2^-$	$27/2^-$	872	68(6)		0.06		14(2)	26	10	
		$25/2^-$	1111	32(6)	2.6(6)	5.7	8.9				
5474	$31/2^-$	$29/2^-$	158	9(3)		1.7		191(67)	690	788	
		$27/2^-$	1030	91(3)	6.5(7)	6.8	8.0				
7527	$(33/2^-)$	$31/2^-$	1753	100		0.09		$\geqslant$0.54	19	10	
7063	$(35/2_1^-)$	$31/2^-$	1289	100	$\geqslant$4.5	0.01	0.02				
7681	$(35/2_2^-)$	$31/2^-$	1907	100	$\geqslant$0.31	0.01	0.02				
8308	$(35/2_3^-)$	$31/2^-$	2534	100	$\geqslant$0.15		0.11				

[a] $B(M2)$ value in Weisskopf units (W.u.).

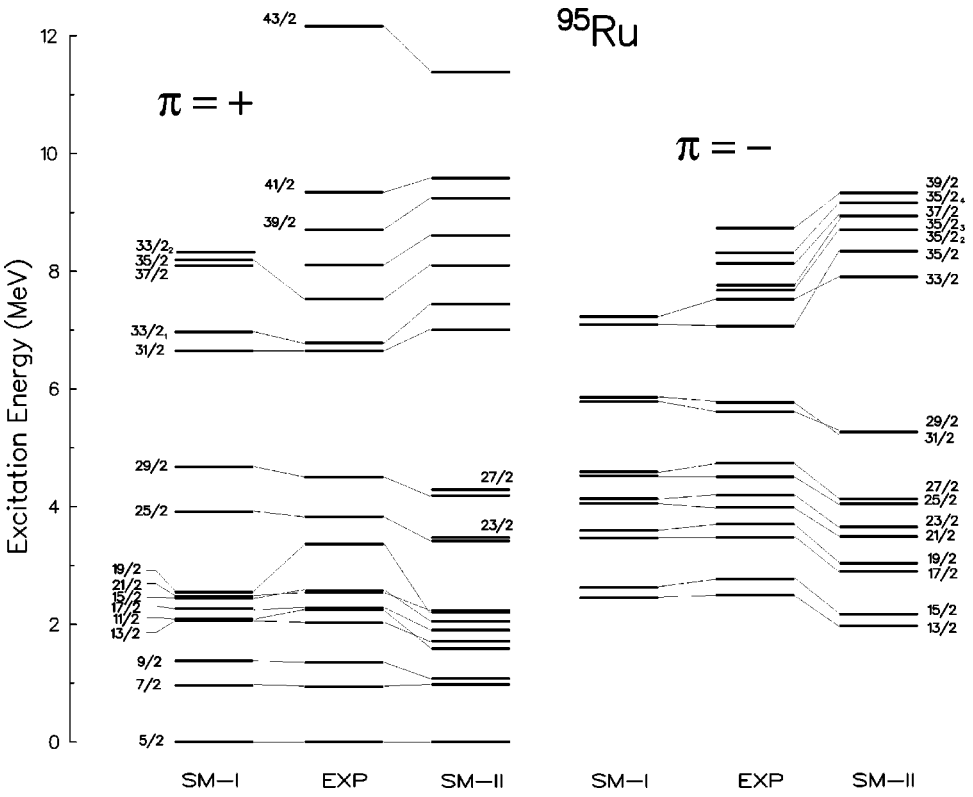

FIG. 10. Experimental and shell-model calculated excitation energies at both parities in ^{95}Ru.

suggest positive parity for the 2247-keV $11/2$ state. Figure 10 illustrates as well the measured and calculated sequence in the negative parity from $13/2^-$ to $35/2^-$. In this case the calculations reproduce the order of the sequence. The energy gap between the 5774-keV $31/2^-$ state and higher spins is reproduced, too. It is interesting to note that the maximum experimental spins correspond to the highest values possible for the model space used in the present calculation.

Figures 11 and 12 compare the experimental and calculated $B(E2)$ transition strengths (see also Table II). The $B(E2)$ values of the $29/2^+$-$17/2^+$ cascade are in the range 1–10 W.u. and for the $(33/2^+)$-$29/2^+$ transition (gap 2), the calculation overemphasizes the decrease in $E2$ strength and places $B(E2)$ below the experimental limit. At negative parity, the $B(E2)$ values range up to ~20 W.u. and, again, the calculation overemphasizes gap 4 (from $35/2^-$ to $31/2^-$). In this calculation, all states other than the $33/2^-$ and $35/2^-$ have more than 90% $\nu(d_{5/2})$ character, while the $33/2^-$ and $35/2^-$ states are almost entirely of $\nu(h_{11/2})$ character.

Continuing at negative parity, a very interesting staggering of $M1$ strengths in the range between 0 and 600 mW.u. is observed (see Fig. 13). The SM-I calculation reproduces this fact, but exaggerates the peak values of the $M1$ decays of the $31/2^-$, $27/2^-$, $23/2^-$, $19/2^-$, and $15/2^-$ levels. An explanation for this staggering can be found looking at the main

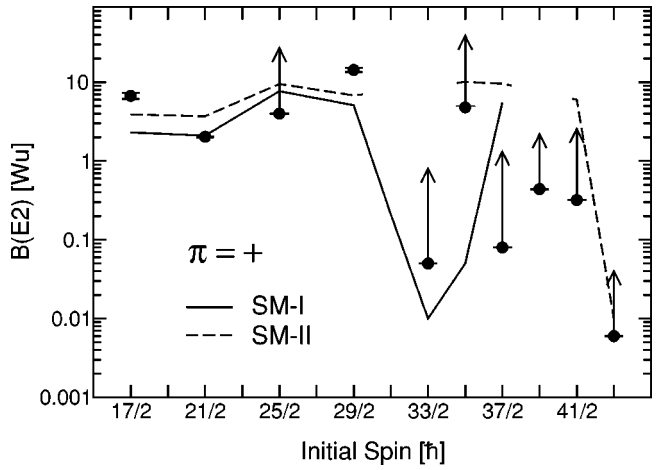

FIG. 11. $B(E2)$ values at positive parity. Only the strengths for $\Delta I=2$ transitions were considered. The value at spin $39/2$ is for the $39/2_2^+ \rightarrow 35/2^+$ transition. The continuous line corresponds to the SM-I calculation and the dashed line to SM-II.

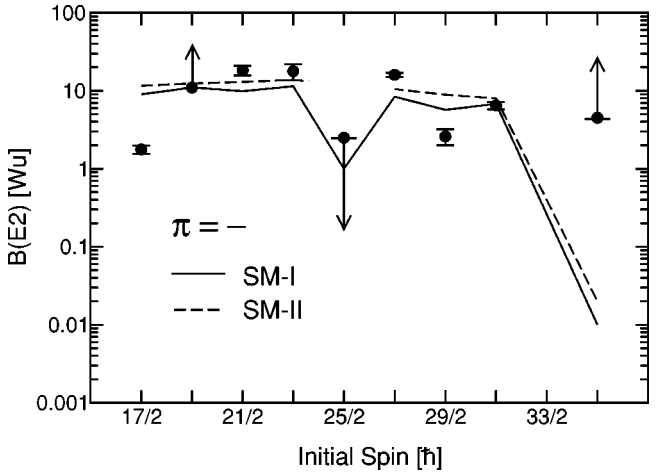

FIG. 12. $E2$ transition strengths at negative parity. Only the strengths for $\Delta I=2$ transitions are considered. The continuous line corresponds to the SM-I calculation and the dashed line to SM-II.

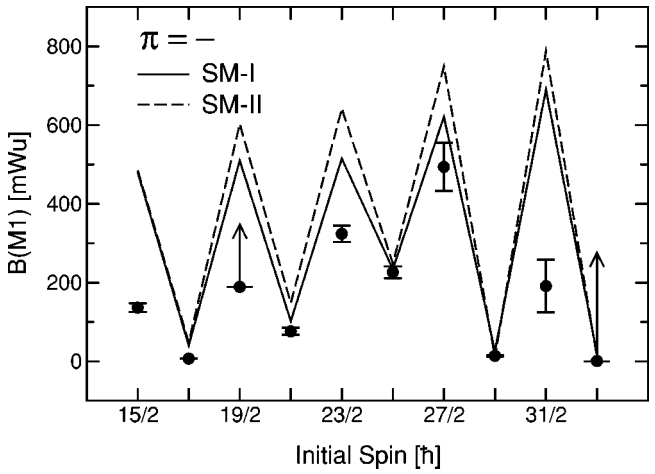

FIG. 13. $M1$ transition strengths at negative parity. Note the staggering which is rather well reproduced by the shell-model calculations in most cases. The continuous line corresponds to the SM-I calculation and the dashed line to SM-II.

partitions of the wave functions displayed in Table III. At negative parity, spins up to $31/2^-$ can be generated with just a $p_{1/2} \rightarrow g_{9/2}$ proton excitation: $\pi(p_{1/2})\pi^5(g_{9/2}) \otimes \nu(d_{5/2}), v_\pi \leqslant 6, v_\nu = 1$. Furthermore, the wave function for the spin $33/2^-$ state is then almost entirely $\pi^4(g_{9/2}) \otimes \nu(h_{11/2}), v_\pi = 4, v_\nu = 1$. The $M1$ transition to the $31/2^-$ state should vanish because the $h_{11/2} \rightarrow d_{5/2}$ single-neutron $M1$ transition is forbidden. The 158-keV transition connects the $31/2^-$ and $29/2^-$ states having identical main configurations (seniority $v=7$) and therefore the $M1$ transition is strongly favored. The wave functions of the $29/2^-$ and $27/2^-$ states, despite being of the same $\pi(p_{1/2})\pi^5(g_{9/2}) \otimes \nu(d_{5/2})$ partition, have proton components with different spins $J_\pi = 13$ and $J_\pi = 11$, respectively, and consequently are not connected by an allowed $M1$ transition. As the wave functions of the states in the spin range from $29/2^-$ to $13/2^-$ have the same structure, $[\pi(p_{1/2})\pi^3(g_{9/2})]_{J_\pi} \otimes \nu(d_{5/2})$ with $J_\pi = 5-13$ and seniorities $v=3$ (up to $I^\pi = 15/2^-$), $v=5$ (up to $27/2^-$), and $v=7$ (up to $31/2^-$), strong and very weak $M1$ transitions alternate with each other and lead to the pronounced staggering of $B(M1)$ illustrated in Fig. 13.

TABLE III. Largest components of the SM-I wave functions of high-spin states in ^{95}Ru at negative parity. The notation $\underline{\pi} \equiv \pi(p_{1/2})$, $\pi \equiv \pi(g_{9/2})$, $\nu \equiv \nu(d_{5/2})$, and $\overline{\nu} \equiv \nu(h_{11/2})$ is used.

E_x (keV)	I^π	Wave function	v	Partition (%)
2493	$13/2^-$	$(\underline{\pi}\pi)_5 \otimes \nu$	3	68
		$(\underline{\pi}\pi)_4 \otimes \nu$	3	20
		$(\underline{\pi}\pi^3)_7 \otimes \nu$	5	6
2774	$15/2^-$	$(\underline{\pi}\pi)_5 \otimes \nu$	3	86
		$(\underline{\pi}\pi^3)_7 \otimes \nu$	5	8
3478	$17/2^-$	$(\underline{\pi}\pi^3)_7 \otimes \nu$	5	59
		$(\underline{\pi}\pi^3)_6 \otimes \nu$	5	26
		$(\underline{\pi}\pi^3)_9 \otimes \nu$	5	11
3702	$19/2^-$	$(\underline{\pi}\pi^3)_7 \otimes \nu$	5	81
		$(\underline{\pi}\pi^3)_9 \otimes \nu$	5	16
3985	$21/2^-$	$(\underline{\pi}\pi^3)_9 \otimes \nu$	5	50
		$(\underline{\pi}\pi^3)_8 \otimes \nu$	5	35
		$(\underline{\pi}\pi^3)_{11} \otimes \nu$	5	12
4192	$23/2^-$	$(\underline{\pi}\pi^3)_9 \otimes \nu$	5	81
		$(\underline{\pi}\pi^3)_{11} \otimes \nu$	5	16
4505	$25/2^-$	$(\underline{\pi}\pi^3)_{11} \otimes \nu$	5	81
4744	$27/2^-$	$(\underline{\pi}\pi^3)_{11} \otimes \nu$	5	94
5616	$29/2^-$	$(\underline{\pi}\pi^5)_{13} \otimes \nu$	7	91
5774	$31/2^-$	$(\underline{\pi}\pi^5)_{13} \otimes \nu$	7	98
7527	$33/2^-$	$\pi^4_{12} \otimes \underline{\nu}(h_{11/2})$	5	98

Although the present calculations provide good information about the states up to spin $29/2^+$ and $31/2^-$ and also appear to illustrate the importance of the $h_{11/2}$ orbital, they do not explain the possible competition of class (a), (b), and (c) mechanisms. Evidently, more realistic calculations need to include such additional excitations. Furthermore, the present calculation does not extend to the next gaps which would highlight the evolution of seniority and the competition of nucleon excitations.

C. The shell-model calculations SM-II

A second set of calculations in ^{95}Ru (referred to as SM-II in the following) was undertaken considering just this $g_{9/2} \rightarrow d_{5/2}, g_{7/2}$ single-neutron excitation. The model space used in these calculations includes the active proton orbitals $\pi(0f_{5/2}, 1p_{3/2}, 1p_{1/2}, 0g_{9/2})$ and neutron orbitals $\nu(0g_{9/2}, 1d_{5/2}, 0g_{7/2})$ relative to a hypothetic ^{68}Ni core. Since a complete set of empirical effective interactions for this model space is not available up to now, various empirical interactions have been combined with results of schematic nuclear interactions applying the surface δ interaction. Details of this procedure are described in our previous shell-model studies of nuclei with $N=48$ [13,14], $N=49$ [15,16], $N=50$ [15,17,18,1,2], $N=51,52$ [19], and $N=53,54$ [20].

The single-particle energies relative to the ^{68}Ni core have been derived from the single-particle energies of the proton orbitals given in Ref. [21] with respect to the ^{78}Ni core and from the neutron single-hole energies of the $1p_{1/2}, 0g_{9/2}$ orbitals [22]. The transformation of these single-particle energies to those relative to the ^{68}Ni core has been performed [23] on the basis of the effective residual interactions given in, e.g., Refs. [15,16]. The obtained values are $\epsilon^\pi_{0f_{5/2}} = -9.806$ MeV, $\epsilon^\pi_{1p_{3/2}} = -9.733$ MeV, $\epsilon^\pi_{1p_{1/2}} = -7.427$ MeV, $\epsilon^\pi_{0g_{9/2}} = -1.227$ MeV, $\epsilon^\nu_{0g_{9/2}} = -6.582$ MeV, $\epsilon^\nu_{1d_{5/2}} = -4.395$ MeV, and $\epsilon^\nu_{0g_{7/2}} = -0.623$ MeV. As found in a similar way in the shell-model studies of the neighboring nuclei ^{94}Ru [2] and ^{95}Rh [1], the reproduction of level energies for states with $J \geqslant 31/2$ in ^{95}Ru could be considerably improved by reducing the neutron $d_{5/2}$ single-particle energy by 1 MeV. Therefore, we present in the following results obtained by using the value $\epsilon^\nu_{1d_{5/2}} = -5.395$ MeV instead of the value given above.

The nucleus ^{95}Ru has 16 protons and 11 neutrons in the considered configuration space. To make the calculations feasible a truncation of the occupation numbers was applied.

The number of protons in the $(1p_{1/2}, 0g_{9/2})$ subshell has been kept to six. One neutron can be lifted from the $0g_{9/2}$ orbital to either the $1d_{5/2}$ or the $0g_{7/2}$ orbital. With these restrictions, configuration spaces with dimensions smaller than 1630 were obtained. The maximum spins reachable in these conditions are $45/2^+$ and $47/2^-$.

The calculated level energies are displayed in Fig. 10 in comparison with the experimental values and with the SM-I calculations. It is interesting to note that the excitation energies at positive parity exhibit some differences in the level ordering. The calculation overestimates gap 2 by $\approx$600 keV whereas it reduces gap 3 to about 2 MeV. The predicted wave functions of the $41/2^+$ and $43/2^+$ yrast states are mainly $\pi^4(g_{9/2}) \otimes \nu^{-1}(g_{9/2})\nu^2(d_{5/2})$ and $\pi^4(g_{9/2}) \otimes \nu^{-1}(g_{9/2})\nu(d_{5/2})\nu(g_{7/2})$, and the gap arises from the $g_{9/2} \rightarrow d_{5/2}, g_{7/2}$ neutron excitation (class *B*). A large difference occurs in the structure of the $33/2^-$ state, for which SM-I predicts a large $\pi^4(g_{9/2}) \otimes \nu(h_{11/2})$, $v=5$ partition (*C*), while SM-II predicts a rather mixed configuration with the $v=9$, $\pi(p_{1/2})\pi^5(g_{9/2}) \otimes \nu^{-1}(g_{9/2})\nu^2(d_{5/2})$ (*B*) partition being largest (but only 28%). Note that this structure prevails up to spin $39/2^-$ (see Table IV). The overall agreement of SM-II with the experimental level energies is somewhat worse than that of SM-I.

In Table II and Figs. 11–13 the calculated transition strengths are compared with the experimental ones and the SM-I calculations. It is rewarding to see that SM-I and SM-II predict very similar $B(E2)$ and $B(M1)$ values and also generally reproduce the inhibitions caused by seniority selection rules, as shown in Figs. 11–13. Another point to note is the qualitative description of the staggering of $B(M1)$ values. Here, the agreement of the data with the SM-I calculations is slightly better than with the SM-II calculations. However, the measured $M1$ strengths $B(M1, 31/2^- \rightarrow 29/2^-) = 191(67)$ mW.u. and $B(M1, 33/2^- \rightarrow 31/2^-) \geq 0.54$ mW.u., which originate from different main configurations in the two calculations, do not allow a distinction between the SM-I and SM-II calculations (see Table II).

V. CONCLUSIONS

The present work extends experimental information on the yrast and yrare states in ^{95}Ru up to 12.2 MeV excitation energy and probable spin $(43/2^+)$. A large number of lifetimes and lifetime limits was determined via RDDS and DDCM, providing information on many $E1$, $E2$, and $M1$ transition strengths.

The levels can be roughly grouped into four substructures separated by high energy transitions of some 1.8–3.5 MeV. At positive parity the lowest structure extends via stretched $E2$ transitions up to spin $29/2^+$. A second structure of parallel stretched $\Delta I=1$ and $\Delta I=2$ transitions covers the spin range $(31/2^+) \leqslant I^\pi \leqslant (41/2^+)$. At negative parity, parallel stretched $\Delta I=1$ and $\Delta I=2$ cascades cover the spin range $13/2^- \leqslant I^\pi \leqslant 31/2^-$, above which four parallel cascades develop, reaching up to $I^\pi=(37/2^-)$.

A qualitative explanation within the shell model interprets these clearly separated structures as due to successive spin couplings of the configuration $\pi^4(g_{9/2}) \otimes \nu(d_{5/2}), I^\pi \leqslant 29/2^+$ and $\pi(p_{1/2})\pi^5(g_{9/2}) \otimes \nu(d_{5/2}), I^\pi \leqslant 31/2^-$. Configurations of higher spin and seniority can be generated by either a $f_{5/2} \rightarrow g_{9/2}$ single-proton excitation $(I^\pi \leqslant 31/2^-, 37/2^+)$, a $d_{5/2} \rightarrow h_{11/2}$ single-neutron excitation $(I^\pi \leqslant 35/2^-, 37/2^+)$, or a $g_{9/2} \rightarrow d_{5/2}, g_{7/2}$ single-neutron-core excitation $(I^\pi \leqslant 41/2^+, 43/2^-)$.

TABLE IV. Main components of wave functions of states in ^{95}Ru (SM-II). The notation $\underline{\pi} \equiv \pi(p_{1/2})$, $\pi \equiv \pi(g_{9/2})$, $\underline{\nu} \equiv \nu^{-1}(g_{9/2})$, $\nu \equiv \nu(d_{5/2})$, and $\nu' \equiv \nu(g_{7/2})$ is used.

I^π	Configuration	Partition (%)
Positive parity		
$5/2^+$	ν	71
$7/2^+$	$\pi^4 \otimes \nu$	74
$9/2^+$	$\pi^4 \otimes \nu$	64
$11/2^+$	$\pi^4 \otimes \nu$	64
$13/2^+$	$\pi^4 \otimes \nu$	52
$15/2^+$	$\pi^4 \otimes \nu$	75
$17/2^+$	$\pi^4 \otimes \nu$	71
$19/2^+$	$\pi^4 \otimes \nu$	68
$21/2^+$	$\pi^4 \otimes \nu$	87
$23/2^+$	$\pi^4 \otimes \nu$	76
$25/2^+$	$\pi^4 \otimes \nu$	91
$27/2^+$	$\pi^4 \otimes \nu$	93
$29/2^+$	$\pi^4 \otimes \nu$	93
$31/2^+$	$\pi^4 \otimes (\underline{\nu}\nu^2)$	47
$33/2^+$	$\pi^4 \otimes (\underline{\nu}\nu^2)$	26
$35/2^+$	$\pi^4 \otimes (\underline{\nu}\nu^2)$	48
$37/2^+$	$\pi^4 \otimes (\underline{\nu}\nu^2)$	48
$39/2^+$	$\pi^4 \otimes (\underline{\nu}\nu^2)$	88
$41/2^+$	$\pi^4 \otimes (\underline{\nu}\nu^2)$	98
$43/2^+$	$\pi^4 \otimes (\underline{\nu}\nu\nu')$	97
Negative parity		
$13/2^-$	$(\underline{\pi}\pi^5) \otimes \nu$	61
$15/2^-$	$(\underline{\pi}\pi^5) \otimes \nu$	83
$15/2_2^-$	$(\underline{\pi}\pi^5) \otimes \nu$	71
$17/2^-$	$(\underline{\pi}\pi^5) \otimes \nu$	57
$19/2^-$	$(\underline{\pi}\pi^5) \otimes \nu$	74
$21/2^-$	$(\underline{\pi}\pi^5) \otimes \nu$	56
$23/2^-$	$(\underline{\pi}\pi^5) \otimes \nu$	75
$25/2^-$	$(\underline{\pi}\pi^5) \otimes \nu$	86
$27/2^-$	$(\underline{\pi}\pi^5) \otimes \nu$	93
$29/2^-$	$(\underline{\pi}\pi^5) \otimes \nu$	94
$31/2^-$	$(\underline{\pi}\pi^5) \otimes \nu$	94
$33/2^-$	$(\underline{\pi}\pi^5) \otimes (\underline{\nu}\nu^2)$	28
$35/2^-$	$(\underline{\pi}\pi^5) \otimes (\underline{\nu}\nu^2)$	37
$35/2_2^-$	$(\underline{\pi}\pi^5) \otimes (\underline{\nu}\nu^2)$	37
$35/2_3^-$	$(\underline{\pi}\pi^5) \otimes (\underline{\nu}\nu^2)$	32
$35/2_4^-$	$(\underline{\pi}\pi^5) \otimes (\underline{\nu}\nu\nu')$	48
$37/2^-$	$(\underline{\pi}\pi^5) \otimes (\underline{\nu}\nu^2)$	80
$39/2^-$	$(\underline{\pi}\pi^5) \otimes (\underline{\nu}\nu^2)$	79

Quantitative predictions of the level energies and $B(M1)$ and $B(M2)$ values have been obtained from the shell-model calculations employing two different model spaces and parametrizations of the single-particle energies and two-body matrix elements. Both model calculations are generally in reasonable agreement with most of the data, but the level energies show a fairly high sensitivity to the single-particle energies used. For some of the states, the determination of lifetimes has been decisive for fixing the shell-model structures. From the point of view of shell-model theory, the presumably short lifetimes of the states with $I^{\pi}=35/2^{+}-43/2^{+}$, for which only limits have been obtained so far, are most interesting to be measured.

As shown in Fig. 11, for the $33/2_1^+$ state only an upper lifetime limit has been determined. According to the shell-model calculations, this state is a seniority isomer, and it would be very desirable to measure the $33/2^{+}\rightarrow 29/2^{+}$ $E2$ transition strength and not only its lower limit.

ACKNOWLEDGMENTS

The authors are most grateful to the crew operating the XTU tandem at Legnaro and the hospitality, which LNL granted them. This work was supported by Deutsches Bundesministerium für Bildung und Forschung and the European Commission within the Contract No. HPRI-1999-CT-00083. A.J. acknowledges financial support from the Deutsche Forschungsgemeinschaft within the Heisenberg program.

[1] A. Jungclaus, D. Kast, K. P. Lieb, C. Teich, M. Weiszflog, T. Härtlein, C. Ender, F. Köck, D. Schwalm, J. Reif, R. Peusquens, A. Dewald, J. Eberth, H. G. Thomas, M. Gorska, and H. Grawe, Nucl. Phys. **A637**, 346 (1998).
[2] A. Jungclaus, D. Kast, K. P. Lieb, C. Teich, M. Weiszflog, T. Härtlein, C. Ender, F. Köck, D. Schwalm, I. P. Johnstone, J. Reif, R. Peusquens, A. Dewald, J. Eberth, H. G. Thomas, M. Gorska, and H. Grawe, Phys. Rev. C **60**, 014309 (1999).
[3] M. Hausmann, A. Jungclaus, E. Galindo, K. P. Lieb, O. Yordanov, I. P. Johnstone, R. Schwengner, A. Dewald, A. Fitzler, O. Möller, G. de Angelis, A. Gadea, T. Martinez, D. R. Napoli, and C. Ur, Phys. Rev. C **68**, 024309 (2003).
[4] S. S. Ghugre *et al.*, Phys. Rev. C **50**, 1346 (1994).
[5] G. Böhm *et al.*, Nucl. Instrum. Methods Phys. Res. A **329**, 248 (1993).
[6] A. Dewald, S. Harrisopulos, and P. von Brentano, Z. Phys. A **334**, 163 (1989).
[7] B. A. Brown and B. H. Wildenthal, Annu. Rev. Nucl. Part. Sci. **38**, 29 (1988).
[8] G. H. Gloeckner and F. J. D. Serduke, Nucl. Phys. **A220**, 477 (1974).
[9] A. Jungclaus, D. Kast, K. P. Lieb, C. Lingk, C. Teich, O. Yordanov, T. Härtlein, P. Reiter, D. Schwalm, I. P. Johnstone, and R. Schwengner, Eur. Phys. J. A **6**, 29 (1999).
[10] I. Johnstone, Phys. Rev. C **44**, 1476 (1991).
[11] S. Perez, Nucl. Phys. **A136**, 599 (1969).
[12] I. Johnstone, Phys. Rev. C **57**, 994 (1998).
[13] R. Schwengner, G. Winter, J. Reif, H. Prade, L. Käubler, R. Wirowski, N. Nicolay, S. Albers, S. Eßer, P. von Brentano, and W. Andrejtscheff, Nucl. Phys. **A584**, 159 (1995).
[14] R. Schwengner, J. Reif, H. Schnare, G. Winter, T. Servene, L. Käubler, H. Prade, M. Wilhelm, A. Fitzler, S. Kasemann, E. Radermacher, and P. von Brentano, Phys. Rev. C **57**, 2892 (1998).
[15] G. Winter, R. Schwengner, J. Reif, H. Prade, L. Funke, R. Wirowski, N. Nicolay, A. Dewald, P. von Brentano, H. Grawe, and R. Schubart, Phys. Rev. C **48**, 1010 (1993).
[16] G. Winter, R. Schwengner, J. Reif, H. Prade, J. Döring, R. Wirowski, N. Nicolay, P. von Brentano, H. Grawe, and R. Schubart, Phys. Rev. C **49**, 2427 (1994).
[17] J. Reif, G. Winter, R. Schwengner, H. Prade, and L. Käubler, Nucl. Phys. **A587**, 449 (1995).
[18] E. A. Stefanova, R. Schwengner, J. Reif, H. Schnare, F. Dönau, M. Wilhelm, A. Fitzler, S. Kasemann, P. von Brentano, and W. Andrejtscheff, Phys. Rev. C **62**, 054314 (2000).
[19] E. A. Stefanova, R. Schwengner, G. Rainovski, K. D. Schilling, A. Wagner, F. Dönau, E. Galindo, A. Jungclaus, K. P. Lieb, O. Thelen, J. Eberth, D. R. Napoli, C. A. Ur, G. de Angelis, M. Axiotis, A. Gadea, N. Marginean, T. Martinez, Th. Kröll, and T. Kutsarova, Phys. Rev. C **63**, 064315 (2001).
[20] E. A. Stefanova, M. Danchev, R. Schwengner, D. L. Balabanski, M. P. Carpenter, M. Djongolov, S. M. Fischer, D. J. Hartley, R. V. F. Janssens, W. F. Mueller, D. Nisius, W. Reviol, L. L. Riedinger, and O. Zeidan, Phys. Rev. C **65**, 034323 (2002).
[21] X. Ji and B. H. Wildenthal, Phys. Rev. C **37**, 1256 (1988).
[22] R. Gross and A. Frenkel, Nucl. Phys. **A267**, 85 (1976).
[23] J. Blomqvist and L. Rydström, Phys. Scr. **31**, 31 (1985).